One-Step Synthesis of Visible Range Luminescent Multicomponent Semiconductor Composites Based on Graphitic Carbon Nitride

Eugene B. Chubenko,* Alexey V. Baglov, and Victor E. Borisenko

Using ternary g-C$_3$N$_4$/ZnO/ZnS bulk composites as an example, it is demonstrated that g-C$_3$N$_4$-based heterojunction systems can be synthesized in a one-step process by pyrolytic decomposition of a mechanical mixture of only two chemical precursors, i.e., thiourea and zinc acetate dehydrate, at 500–625 °C with subsequent in situ interaction and polymerization of the products. Scanning electron microscopy (SEM), energy-dispersive X-ray spectroscopy (EDX), X-ray diffraction (XRD), and X-ray photoelectron spectroscopy (XPS) analyses reveal that the synthesized composites consist of intermixed alloyed g-C$_3$N$_4$, ZnO, and ZnS grains with good crystalline quality. The materials demonstrate bright photoluminescence (PL) at room temperature in the photon energy range of 1.5–3.0 eV (410–800 nm) which can be tuned by the synthesis temperature. A phase sequence during the synthesis and peculiarities of the PL are discussed.

1. Introduction

Graphitic carbon nitride (g-C$_3$N$_4$) started to be thoroughly studied in recent decade because of its photocatalytic properties[1,2] and promising potential for production of hydrogen and hydrocarbon fuel.[3] An effective light absorption in the visible range makes this organic semiconductor ($E_g = 2.70$–2.88 eV room temperature)[1,2] to be very attractive for combination with wide bandgap inorganic semiconductors to get an increased photocatalytic activity supposing Z-scheme transfer of photogenerated charge carriers in composite heterostructures which could be also useful for novel light-emitting devices.[4] However, the synthesis of g-C$_3$N$_4$ heterojunction systems usually consists of

multiple steps intended to construct multi-layered or core–shell-like structures and includes many intermediate operations.

Fabrication of composites based on g-C$_3$N$_4$ and wide bandgap semiconductors is a reasonable strategy to achieve good catalytic performance of the materials without using expensive noble or rare metals.[2,5] Energy positions of conduction band (CB) and valence band (VB) edges in ZnO, TiO$_2$, ZrO$_2$, ZnS, SiC, and some ternary semiconductor compounds at normal pH is "lucky" enough to maintain efficient heterogeneous photocatalysis.[6] Meanwhile, photocatalysis is not the only application area for g-C$_3$N$_4$. Scientific community in a pursuit of perfect photocatalyst almost ignored using g-C$_3$N$_4$ as a light-emitting material despite its bright wide range luminescence. There are some attempts undertaken to fabricate white light-emitting devices using this material as a luminophore, combining it with oxides (silica),[7] semiconductors (ZnO),[8] phosphorus (Y$_2$MoO$_6$:Eu^{3+}),[9] and organic compounds (2-aminothiophene-3-carbonitrile).[10]

Both in the attempts to obtain efficient photocatalytic coatings or light-emitting devices to unleash the potential of g-C$_3$N$_4$ fabrication of multicomponent systems consisting of g-C$_3$N$_4$ itself and complimentary wide bandgap semiconductors are needed. Semiconducting ZnO ($E_g = 3.37$ eV)[6] and ZnS ($E_g = 3.54$ eV)[6] suit well to construct binary or ternary heterogeneous systems including g-C$_3$N$_4$. Among others such composites were claimed to possess better photocatalytic and photovoltaic properties.[1,11,12] Meanwhile note that the proposed fabrication process is complicated and time consuming: each compound was synthesized individually and then they were mixed to obtain semiconductor particles decorated with g-C$_3$N$_4$ flakes.[11,12] Moreover, the produced composites have remained poorly studied.

Herein, we describe a new facile approach for synthesis of ternary g-C$_3$N$_4$-based heterojunction composites promoting our previous experimental techniques.[13–15] It exploits the idea to synthesize interconnecting g-C$_3$N$_4$, semiconducting metal oxide and metal sulfide by pyrolytic decomposition of thiourea and metal acetate in their mixture followed by in situ chemical interaction and polymerization of the products. Thiourea provides tri-s-triazine units for construction of g-C$_3$N$_4$ polymer and sulfur for the formation of the metal sulfide, whereas the metal acetate serves as a metal source. Oxygen comes from water vapors. This approach has been tested on an example of g-C$_3$N$_4$/ZnO/ZnS bulk composites synthesized at 500–625 °C and analyzed with

Prof. E. B. Chubenko, A. V. Baglov, Prof. V. E. Borisenko
Department of Micro- and Nanoelectronics
Belarusian State University of Informatics and Radioelectronics
6 P. Brovka street, Minsk 220013, Belarus
E-mail: eugene.chubenko@bsuir.by, eugene.chubenko@gmail.com

Prof. V. E. Borisenko
Department of Physics of Condensed Matter
National Research Nuclear University MEPhI
31 Kashirskoe Shosse, Moscow 115409, Russia

ⓘ The ORCID identification number(s) for the author(s) of this article can be found under https://doi.org/10.1002/adpr.202000004.

**ADVANCED
SCIENCE NEWS**

www.advancedsciencenews.com

**ADVANCED
PHOTONICS
RESEARCH**
Open Access

www.adpr-journal.com

scanning electron microscopy (SEM), energy-dispersive X-ray spectroscopy (EDX), X-ray diffraction (XRD), X-ray photoelectron spectroscopy (XPS) and photoluminescence (PL) techniques.

2. Results and Discussion

SEM images show that the synthesized materials consist of distinguishable interconnected crystal-like grains as large as few micrometers covered by flakes (**Figure 1**) with the surface becoming more porous with the increasing temperature. It can be an indication of an evaporation of the components during thermal processing. The grains have also got better resolved crystalline features at higher temperatures.

The synthesized materials revealed by EDX were found to contain carbon, nitrogen, zinc, sulfur, and oxygen. The C/N atomic ratio is within the range of 0.70–0.84 and slightly increases with the synthesis temperature. Despite the carbon loss[16,17] at high temperatures, it exceeds the nominal g-C_3N_4 stoichiometric value 0.75. Zn/S and Zn/O atomic ratios are above 1.00 in the whole studied temperature range. Concentration of Zn atoms higher than S or O ones points that the composites can include not only ZnO and ZnS but also their ternaries or even metallic Zn as Zn/(S + O) ratio exceeds 1.00 upon synthesis at temperatures above 600 °C.

XRD patterns (**Figure 2**) confirm that crystalline g-C_3N_4, ZnO, and ZnS have been formed in the synthesized material. The band in the range of $2\theta = 12.3°–13.05°$ corresponds to the (210) plane of crystalline g-C_3N_4 with polymerized tri-s-triazine units.[16] Calculated in-plane distance is 6.78 Å for the sample synthesized at 500 °C, and it increases to 7.19 Å for 625 °C sample. Nevertheless, the last value is still smaller than the in-plane distance in perfect g-C_3N_4 which is 7.40 Å.[18] The position of g-C_3N_4 (002) band at $2\theta = 27.65°–28.0°$ corresponds to 3.22–3.18 Å interplane distance between the layers of the polymerized tri-s-triazine monomers which is equal to 3.40 Å in
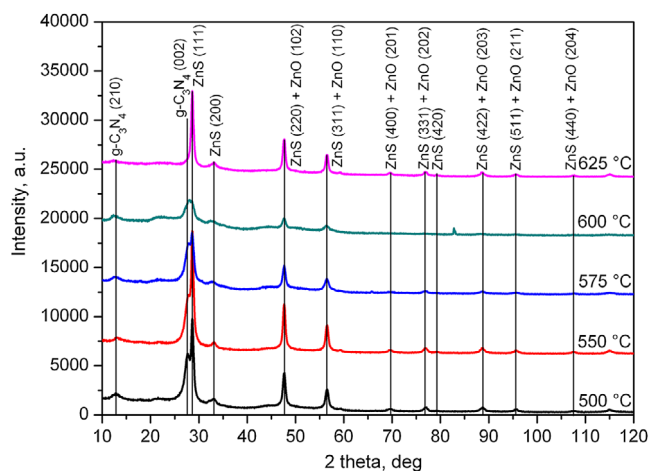

Figure 2. XRD patterns for the composite materials synthesised from the mixture of thiourea and zinc acetate dehydrate at different temperatures. The peaks are identified using International Centre for Diffraction Data database.

perfect g-C_3N_4.[18] Contrary to the in-plane distance, the plane-to-plane distance decreases with the synthesis temperature.

A number of XRD peaks are also identified to belong to crystalline ZnS with a sphalerite lattice and probable to ZnO with a wurtzite lattice. Their positions do not depend on the synthesis temperature. ZnS (111) peak at 28.65° overlaps with g-C_3N_4 (002) one while for the materials synthesis above 600 °C, this signature of g-C_3N_4 becomes barely resolved. It should be noted that three main ZnO (100), (002), and (101) (at 31.8°, 34.4°, and 36.3° correspondingly) phase peaks do not observed at XRD patterns. Also, metallic Zn peaks were not detected by XRD.

XPS spectra of the samples obtained at 550, 575, and 600 °C (**Figure 3**) confirm the presence of g-C_3N_4 in the composite. Carbon 1s electronic shell (C 1s) band consists of three components which can be approximated with Gauss function with
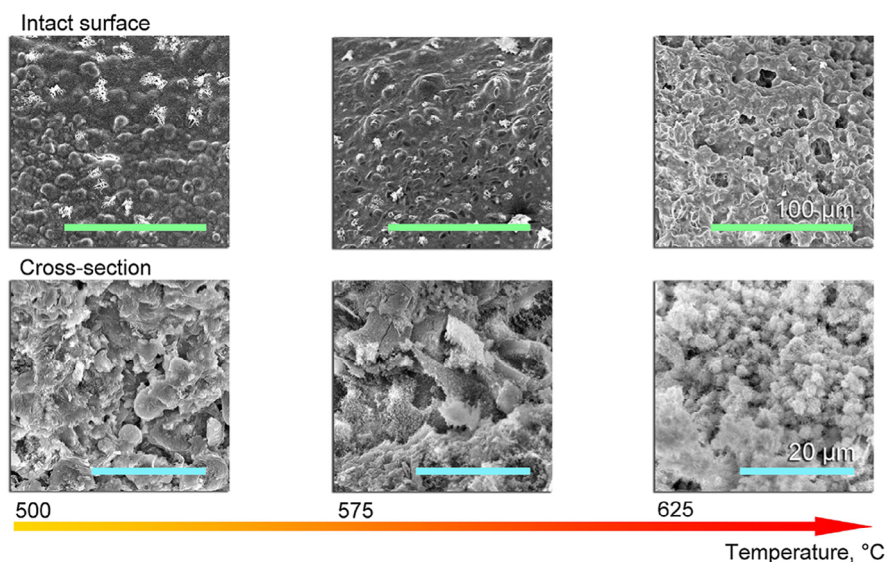

Figure 1. Structure evolution of the composite material synthesised from the mixture of thiourea and zinc acetate dehydrate in the temperature range of 500–625 °C. The scale bars on SEM images are the same for both rows.
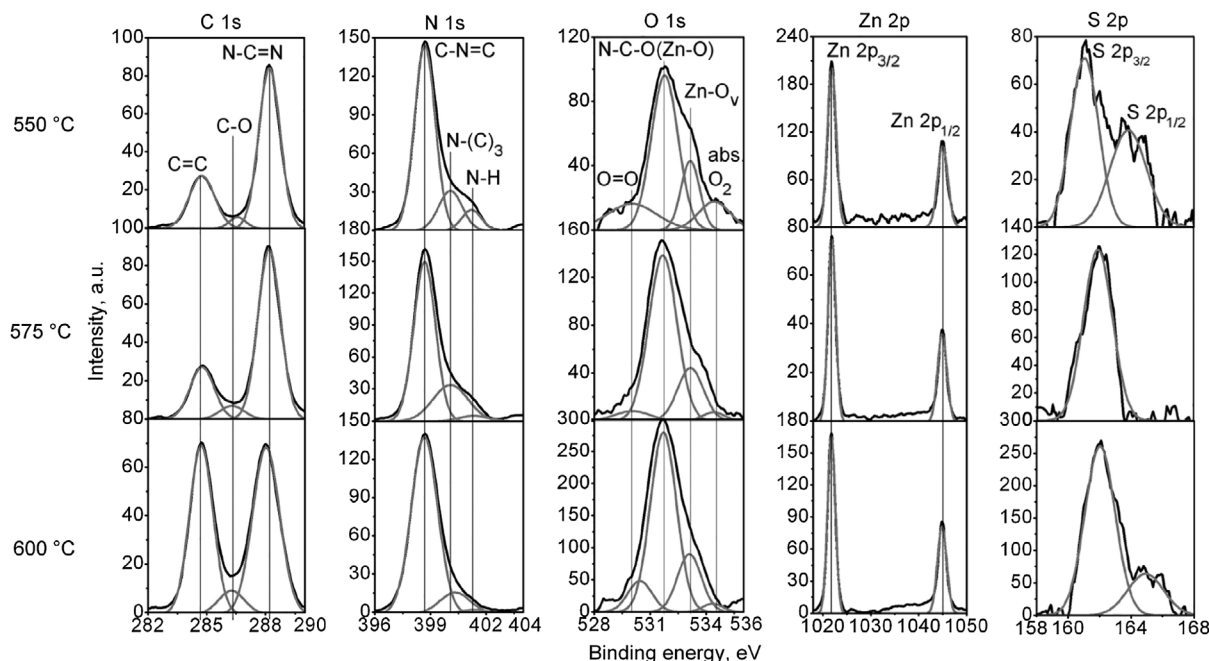
Figure 3. XPS spectra of composite materials synthesized from the mixture of thiourea and zinc acetate dehydrate at different temperatures.

maximum at 284.71, 286.46, and 288.16 eV corresponding to sp^2 C=C double bonds, oxygen C—O, and nitrogen N–C=N sp^2 bonds.[19]

Assymetrical single band, corresponding to nitrogen N 1s bonds, consists of three band typical for g-C$_3$N$_4$: carbon C—N=C bond (maximum at 398.6 eV), nitrogen atoms surrounded by three carbon atoms N—(C)$_3$ (at 400.1 eV) and residual amines in the g-C$_3$N$_4$ crystal structure (401.3 eV).[19] Analysis of O 1s band is more complicated. We identified at least four bands corresponding to oxygen double O=O bonds (530.02 eV), N—C—O groups (532.75 eV) possibly overlapping with oxygen in ZnO crystal lattice (Zn—O), oxygen vacancies in ZnO band (Zn—O$_v$) (at 533.15 eV), and to oxygen and water absorbed at the surface (abs. O$_2$ in Figure 3) with maximum at 534.5 eV.[19–21] Zn 2p region of XPS spectra contain splitted band typical for ZnS and ZnO with maximums at 1022.0 and 1045.1 eV corresponding to Zn 2p$_{3/2}$ and Zn 2p$_{1/2}$ states.[20–22] Low-intensity sulfur S 2p band are presented on all XPS spectra. Two splitted lines S 2p$_{3/2}$ and S 2p$_{1/2}$ with maximum at 161.0 and 163.8 eV can be identified here.[22]

The synthesized ternary g-C$_3$N$_4$/ZnO/ZnS composites demonstrate bright room temperature luminescence under ultraviolet (UV) excitation (**Figure 4**). Their PL spectra significantly change as a function of the synthesis temperature while wide visible range (1.5–3.0 eV) is always covered. The PL intensity maximum shifts from 2.68 eV (blue range) for the composite synthesized at 500 °C to 2.15 eV (orange range) for 625 °C sample. In general, the spectra contain two distinct broad bands, the peak intensities of which compete with each other in the synthesis temperature range. The band at high energies (3.0–2.2 eV) attributed to recombination processes in g-C$_3$N$_4$[1,2,7,10] shifts to the lower energy range with the increase in the synthesis temperature. Another energy band at low energies (2.4–1.8 eV) is

considered as a fingerprint of crystal lattice defects in ZnO and/or ZnS.[23,24] The intensity of the g-C$_3$N$_4$-related band at the synthesis temperatures above 575 °C drops below the intensity of the ZnO/ZnS band which at the same time sharply increases with the temperature.

Analyzing the experimental data presented, we suppose the following chemical reactions and phase sequence resulting in the formation of g-C$_3$N$_4$/ZnO/ZnS composites (**Figure 5**).

The studied system initially consists of two precursors, which are thiourea and zinc acetate dehydrate. At ≈180 °C, thiourea melts and decompose to thiocyanic acid (HSCN) or its tautomer isothiocyanic acid (HNCS) releasing free gaseous ammonia (NH$_3^-$).[25] At normal pressure conditions and at the elevated temperature, HSCN is the gaseous compound. Its iso-HNCS form usually dominates in the vapor phase.[26] During the further heating, sulfur-containing species (carbon disulfide [CS$_2$] and hydrogen sulphide [H$_2$S]) split off from HNCS and HSCN before the formation of melamine,[27] evaporates and leaves the quasi-hermetically sealed crucible. Remaining products react with each other and with ammonia originated in the crucible ambient as a result of the thiourea decomposition. At 234 °C, they form melamine. With an increasing temperature, melamine undergoes chain of thermal polymerization reactions and consequently transforms to melam, melem, and at above 300 °C to melon. Finally, at above 420 °C, melon polymerizes to g-C$_3$N$_4$.[16] The melamine → melam → melem → melon reaction chain is not shown in Figure 4 for simplicity.

In parallel to the above transformations, uncalcinated zinc acetate dehydrate (Zn(CH$_3$COO)$_2$·2H$_2$O) begins to lose its water at temperatures above 50 °C and transforms to anhydrous form Zn(CH$_3$COO)$_2$ at ≈100 °C.[28] At that point, it begins to melt. In the temperature range of 150–235 °C, Zn(CH$_3$COO)$_2$ reacts with H$_2$O producing basic zinc acetate (Zn$_4$O(CH$_3$COO)$_6$) and
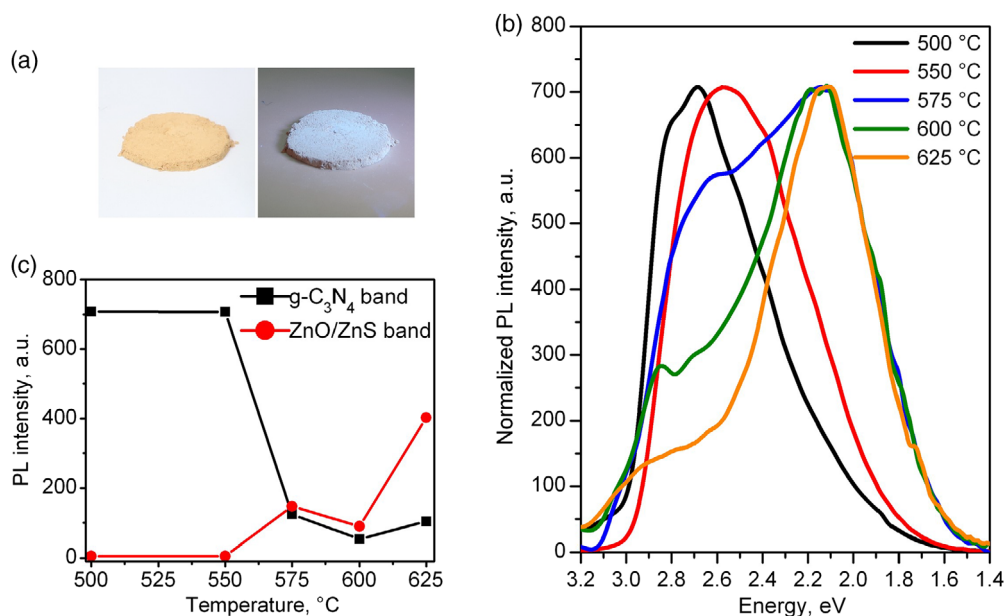
Figure 4. Luminescence of the synthesized g-C_3N_4/ZnO/ZnS composites. a) Composite synthesized at 550 °C under visible light (left) and blue light emission from same material excited by 365 nm UV radiation (right). b) PL spectra of the composites synthesized at different temperatures normalized to their maximum light intensity. c) Integral intensity of the two major bands belonging to g-C_3N_4 and ZnO/ZnS as a function of the synthesis temperature.

releasing acetic acid (CH_3COOH).[28,29] Basic zinc acetate in the temperature range from 270 to 300 °C continues to react with H_2O until all acetic groups become free leaving crystalline ZnO as a residue.[28,29] At higher temperatures, basic zinc acetate can also directly decompose producing solid ZnO and releasing gaseous carbon dioxide (CO_2) and acetone ((CH_3)CO).[29]

In the system containing both thiourea and zinc acetate at above 100 °C, thiourea can react with melted zinc acetate forming $Zn(CH_3COO)_2$–$2NH_2CSNH_2$ complexes. However, if even an existence of such complexes is true they must decompose at above 140 °C releasing thiourea back.[30]

It is known that at temperatures higher than 300 °C, ZnO is becoming thermodynamically more preferable than ZnS. In the case of unlimited supply of oxygen in the ambient atmosphere, sulfur from ZnS reacts with oxygen, producing gaseous sulfur dioxide SO_2 and ZnO.[31] So, ZnS should be completely converted into ZnO at a temperature higher than 500 °C, and all sulfur must be evaporated from the residue.[31] However, in our experiments, the material synthesized at a temperature higher than 550 °C contains high EDX detectable amount of sulfur. Moreover, XRD and XPS detect both ZnS and ZnO crystal phases in the residue. We suppose that in a closed ambient with a limited supplies of oxygen and H_2O vapors sulfur-containing volatile substances (CS_2 and H_2S) react with zinc oxide acetate producing ZnS. It is quite possible as ZnO is easily reacting with acids producing appropriate salts. Oxygen can leak either away from the crucible or become trapped inside g-C_3N_4. After the complete decomposition of zinc acetate, interconnected ZnO/ZnS grains are formed. Meanwhile, a limited amount of oxygen and H_2O in the crucible leaves a certain amount of amorphous unoxidized Zn resulting in an excess of metal atoms in the composite not detected by XRD due to absence of crystal structure.

Formation of ZnO/ZnS and g-C_3N_4 starts almost simultaneously. However, condensation of ZnO/ZnS occurs at much lower temperature (below 320 °C) as compared with the polymerization temperature of g-C_3N_4 (450–500 °C). Thus, we suppose that in our case g-C_3N_4 is polymerized on the surface of already crystallized ZnO/ZnS grains. The PL spectra of the composites synthesized at 500 and 550 °C demonstrate preferably the band typical for g-C_3N_4 (Figure 4c) because ZnO/ZnS crystallites are shielded by g-C_3N_4. It is also supported by the SEM observation. At higher synthesis temperatures, the balance is changed to ZnO/ZnS.

The observed two major PL bands are considered to be a result of radiative recombination processes in g-C_3N_4 and ZnO/ZnS. To understand their nature, we propose cyclic energy band diagram (**Figure 6**) for the first time including all three possible heterojunctions, i.e., g-C_3N_4/ZnO, g-C_3N_4/ZnS, and ZnO/ZnS, performing in an ensemble. It has been designed using the Anderson rule[32] supposing that electron energy levels of the contacting materials are lined up in vacuum according to their electron affinities. High-energy electron transitions (1)–(5) occur in g-C_3N_4. Its energy band structure is formed by the VB ($E_{V(g-C3N4)}$) controlled by C—N σ-bonds with sp^3-hybridization and C—N π-bonds with sp^2-hybridization. The CB ($E_{C(g-C3N4)}$) is formed by a superposition of excited σ*- and π*-bonds.[33,34] N_2 lone pairs (LPs), oxygen defect, and nitrogen defect are also represented by energy levels in the bandgap of g-C_3N_4.[33,34] Thus, the observed red shift of the luminescence peak intensity at high synthesis temperatures can be reasonably explained by a growing polymerization rate of g-C_3N_4, and its densification confirmed by shortening the interplane distance and decrease in the intensity of XPS spectra band at N 1s range, corresponding to residual NH_3^- groups (Figure 3), gradually splitting off with growing

ADVANCED
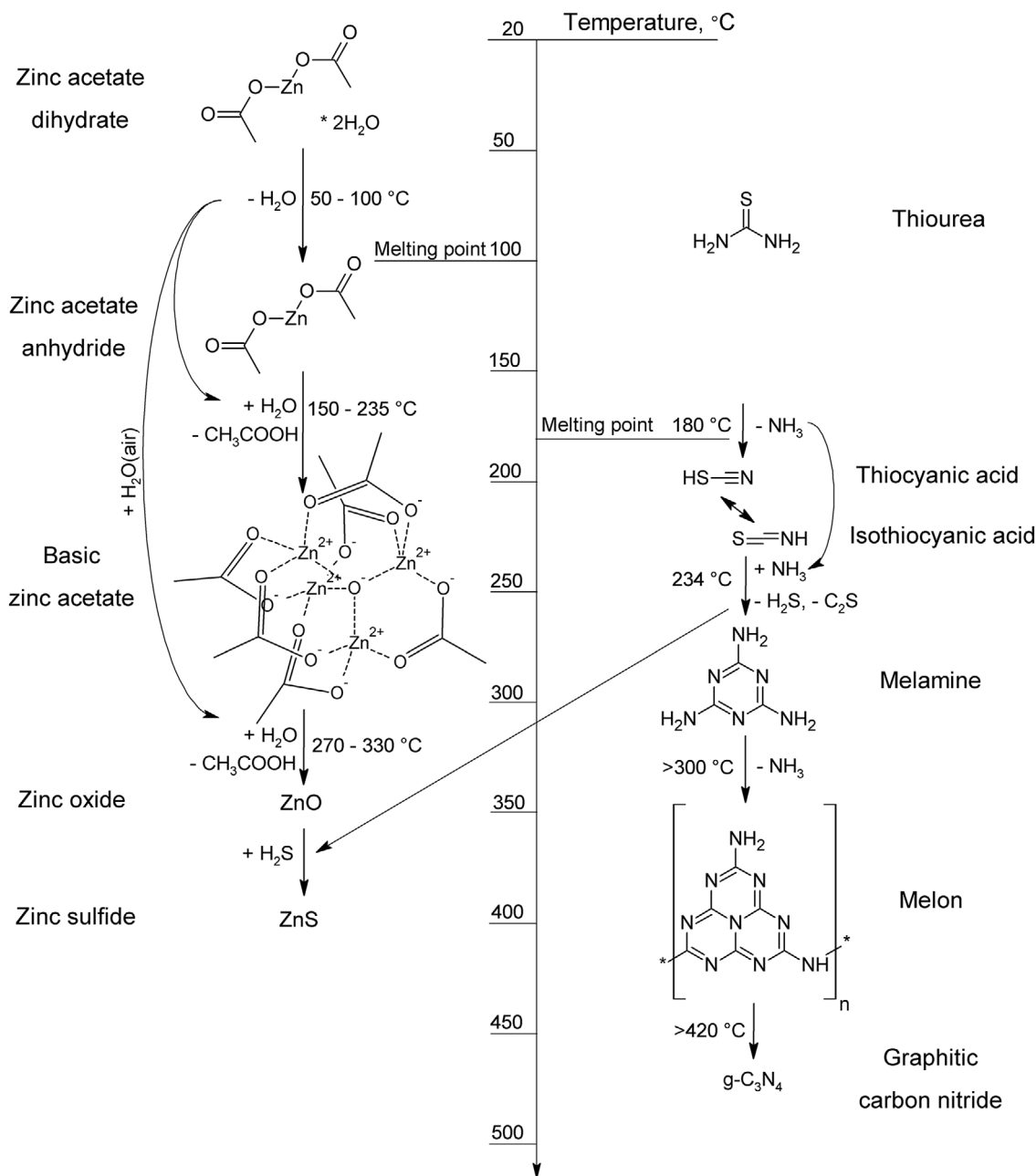SCIENCE NEWS
www.advancedsciencenews.com

ADVANCED
PHOTONICS
RESEARCH
Open Access
www.adpr-journal.com

Figure 5. Synthesis of g-C$_3$N$_4$/ZnO/ZnS composites from the mixture of thiourea and zinc acetate dehydrate.

temperature. Oxygen doping effects are also responsible of luminescence red shift, as g-C$_3$N$_4$ doping with oxygen occurs during polymerization at used synthesis conditions.[14]

However, partial thermal decomposition and evaporation of the already formed g-C$_3$N$_4$ pointed out by the increased in-plane distance results in the decrease in the PL intensity. ZnO usually contains oxygen vacancies (V_O) and interstitial oxygen atoms (O_i) as well as Zn interstitials (Zn_i) giving rise to an appearance of defect energy levels in the bandgap.[23] ZnS can also have defect levels in the bandgap associated with sulfur vacancies (V_S) and interstitial atoms (S_i) and zinc interstitials (Zn_i) and vacancies

(V_{Zn}).[24] So far, electron transitions (5)–(11) in ZnO and ZnS are considered to be responsible for lower-energy PL band observed for g-C$_3$N$_4$/ZnO/ZnS composites. Its maximum does not shift with the synthesis temperature (Figure 2b), suggesting that the nature of the defects also does not change in the studied temperature range.

CB offsets are favorable for a transfer of electrons photogenerated in g-C$_3$N$_4$ to neighboring ZnO and ZnS. Their jumping down to the defect energy levels and subsequent radiative recombination with less mobile holes in these semiconductors extend the spectral range of the emitting light.
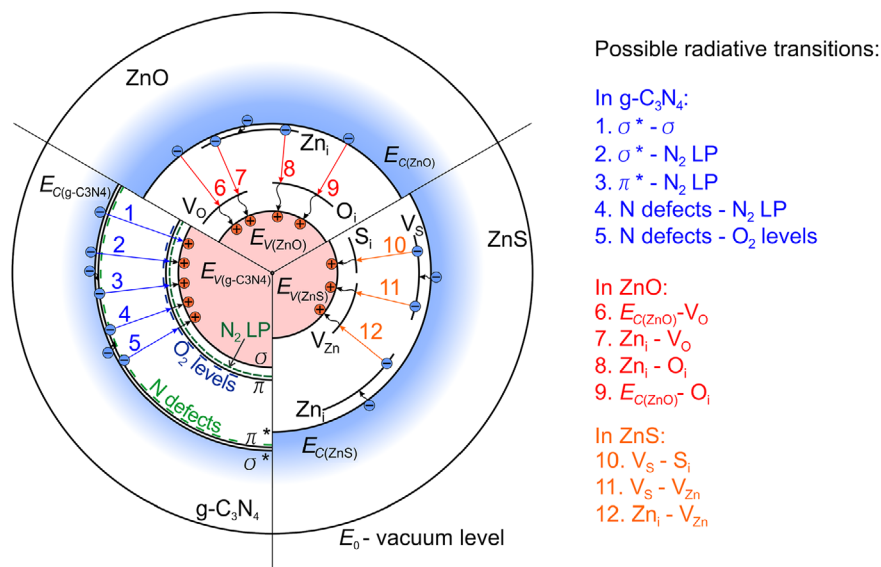
Figure 6. Cyclic energy band diagram of g-C_3N_4/ZnO/ZnS composite.

3. Conclusion

In conclusion, we have proved experimentally that ternary heterojunction composites including g-C_3N_4, semiconducting metal oxide and metal sulfide can be easily one-step fabricated by thermal processing at 500–625 °C of mixed thiourea and metal acetate used as chemical precursors. The synthesized and studied g-C_3N_4/ZnO/ZnS composites have demonstrated good crystallinity of the particular semiconducting components and bright room temperature photoluminescence in the wide visible range. Spectral composition of the emitted light in the photon energy range of 1.5–3.0 eV is determined by radiative transitions in g-C_3N_4 mediating the high energy part of the spectrum and by radiative transitions involving intrinsic point defects in ZnO and ZnS responsible for its low energy part. It gives an opportunity for a spectral design of the composites by the temperature regime of synthesis and/or by changing the mass ratio of the precursors. The demonstrated synthesis approach is believed to be scaled up to a number of other g-C_3N_4/oxide/sulfide systems with different metals, forming semiconducting oxides and sulfides.

4. Experimental Section

The composite materials were synthesized by simultaneous pyrolytic decomposition of chemical precursors with subsequent thermal polymerization of the products. Analytical grade thiourea (CH_4N_2S) and zinc acetate dehydrate ($Zn(CH_3CO_2)_2 \cdot 2H_2O$) were used as the precursors. They were mechanically mixed at 1:1 mass ratio and grounded down to fine powder in an agate mortar. The powder was then loaded into a ceramic crucible and quasihermetically closed there by an aluminum foil. The atmosphere inside the crucible was an ambient air. Aluminum foil sealing allowed gases to come out from closed space but prevented penetration of ambient atmosphere inside the crucible during the process. Crucible was heated at the rate of 5 °C min^{-1} in a muffle furnace to 500–625 °C, kept at the fixed temperature for 30 min and cooled down within 12 h to the room temperature like in our previous experiment.[13–15,35]

Morphology of the synthesized composites was analyzed with scanning electron microscopy (SEM) using Hitachi S–4800 operating at the electron acceleration voltage of 15 kV. Atomic composition of the composites was studied with EDX using Bruker QUANTAX 200 EDX spectrometer. Crystalline phases in the samples were identified by XRD analysis using DRON-4 diffractometer using Cu Kα line ($\lambda = 1.54184$ Å). PL spectra were recorded at room temperature by SOLAR TII MS7504i spectrophotometer equipped with Proscan HS101 CCD camera as a detector. A 1000 W xenon lamp was used to excite PL. Narrow monochromatic lines were cut from the broad spectra of the lamp radiation by double monochromator SOLAR TII DM 160.

Conflict of Interest

The authors declare no conflict of interest.

[1] J. Wen, J. Xie, X. Chen, X. Li, *Appl. Surf. Sci.* **2017**, *391*, 72.

[2] A. Wang, C. Wang, L. Fu, W. Wong-Ng, Y. Lan, *Nano-Micro Lett.* **2017**, *9*, 47.

[3] X. Wang, K. Maeda, A. Thomas, K. Takanabe, G. Xin, J. M. Carlsson, K. Domen, M. Antonietti, *Nat. Mater.* **2009**, *8*, 76.

[4] P. Zhou, J. Yu, M. Jaroniec, *Adv. Mat.* **2014**, *26*, 4920.

[5] Z. Zhao, Y. Sun, F. Dong, *Nanoscale* **2015**, *7*, 15.

[6] A. Hernández-Ramírez, I. Medina-Ramírez, in *Photocatalytic Semiconductors: Synthesis, Characterization, and Environmental Applications* (Eds: A. Hernández-Ramírez, I. Medina-Ramírez), Springer International Publishing, Switzerland **2015**, pp. 1–9.

[7] A. Wang, C. Lee, H. Bian, Z. Li, Y. Zhan, J. He, Y. Wang, J. Lu, Y. Y. Li, *Part. Part. Syst. Charact.* **2017**, *34*, 1600258.

[8] S. Bayan, N. Gogurla, A. Midya, S. K. Ray, *Carbon* **2016**, *108*, 335.

[9] B. Han, Y. Xue, P. Li, J. Zhang, J. Zhang, H. Shi, *J. Solid State Chem.* **2015**, *232*, 26.

[10] Q. Guo, *Adv. Opt. Mater.* **2019**, *2019*, 1900775.

[11] Z. Dong, Y. Wu, N. Thirugnanam, G. Li, *Appl. Surf. Sci.* **2018**, *430*, 293.

[12] C. Liu, Y. Qiu, F. Wang, K. Wang, Q. Liang, *Adv. Mater. Interfaces* **2017**, 1700681.

[13] N. M. Denisov, E. B. Chubenko, V. P. Bondarenko, V. E. Borisenko, *Tech. Phys Lett.* **2019**, *45*, 108.

[14] E. B. Chubenko, N. M. Denisov, A. V. Baglov, V. P. Bondarenko, V. V. Uglov, V. E. Borisenko, *Cryst. Res. Technol.* **2020**, *55*, 1900163.

[15] E. B. Chubenko, A. V. Baglov, E. S. Lisimova, V. E. Borisenko, *Int. J. Nanosci.* **2019**, *18*, 1940042.

[16] B. Jürgens, E. Irran, J. Senker, P. Kroll, H. Müller, W. Schnick, *J. Am. Chem. Soc.* **2003**, *125*, 10288.

[17] A. Thomas, A. Fischer, F. Goettmann, M. Antonietti, J.-O. Müller, R. Schlögl, J. M. Carlsson, *J. Mater. Chem.* **2008**, *18*, 4893.

[18] M. J. Bojdys, J.-O. Miller, M. Antonietti, A. Thomas, *Chem. Eur. J.* **2008**, *14*, 8177.

[19] R. Kumar, M. A. Barakat, F. A. Alseroury, *Sci. Rep.* **2017**, *7*, 12850.

[20] S. Baruah, J. Dutta, *Sci. Technol. Adv. Mater.* **2009**, *10*, 013001.

[21] M. Chen, X. Wang, Y. H. Yu, Z. L. Pei, X. D. Bai, C. Sun, R. F. Huang, L. S. Wen, *Appl. Surf. Sci.* **2000**, *158*, 134.

[22] F. A. La Porta, M. M. Ferrer, Y. V. B. de Santana, C. W. Raubach, V. M. Longo, J. R. Sambrano, E. Longo, J. Andrés, M. S. Li, J. A. Varela, *J. Alloys Compd.* **2013**, *556*, 153.

[23] S. Vempati, J. Mitra, P. Dawson, *Nanoscale Res. Lett.* **2012**, *7*, 470.

[24] X. Wang, J. Shi, Z. Feng, M. Li, C. Li, *Phys. Chem. Chem. Phys.* **2011**, *13*, 4715.

[25] S. C. Moldoveanu, *Pyrolysis of Organic Molecules*, Elsevier Science, Amsterdam **2019**, pp. 697–714.

[26] C. I. Beard, B. P. Dailey, *J. Chem. Phys.* **1950**, *18*, 1437.

[27] G. Zhang, J. Zhang, M. Zhang, X. Wang, *J. Mater. Chem.* **2012**, *22*, 8083.

[28] A. V. Ghule, B. Lo, S.-H. Tzing, K. Ghule, H. Chang, Y. C. Ling, *Chem. Phys. Lett.* **2003**, *381*, 262.

[29] C.-C. Lin, Y.-Y. Li, *Mater. Chem. Phys.* **2009**, *113*, 334.

[30] K. Gydryová, V. Balek, *J. Therm. Anal.* **1993**, *40*, 519.

[31] R. Wahab, S. G. Ansari, Y.-S. Kim, M. S. Dhage, H. K. Seo, M. Song, H.-S. Shin, *Met. Mater. Int.* **2009**, *15*, 453.

[32] V. E. Borisenko, S. Ossicini, *What is What in the Nanoworld*, Wiley-VCH, Weinheim **2012**, p. 10.

[33] B. Choudhury, K. K. Paul, D. Sanyal, A. Hazarika, P. K. Giri, *J. Phys. Chem. C* **2018**, *122*, 9209.

[34] Y. Zhang, Q. Pan, G. Chai, M. Liang, G. Dong, Q. Zhang, J. Qiu, *Sci. Rep.* **2013**, *3*, 1943.

[35] A. V. Baglov, E. B. Chubenko, A. A. Hnitsko, V. E. Borisenko, A. A. Malashevich, V. V. Uglov, *Semiconductors* **2020**, *54*, 226.